Int J Adv Manuf Technol (2016) 87:1957–1965
DOI 10.1007/s00170-016-8583-7

ORIGINAL ARTICLE

Research on surface topography in ultra-precision flycutting based on the dynamic performance of machine tool spindle

Xu Yang[1,2] · Chenhui An[1] · Zhenzhong Wang[2] · Quanjin Wang[2] · Yunfeng Peng[2] · Jian Wang[1]

Received: 23 November 2015 / Accepted: 2 March 2016 / Published online: 14 March 2016

Abstract The dynamic performance of ultra-precision cutting machine tools is an important factor for its machining accuracy. To improve the precision of the machine tool, a surface topography model is built in this paper and the tool path during the cutting process is achieved by dynamic finite element analysis (DFEA) of the air spindle in ANSYS, surface topography is obtained using MATLAB simulation by combing the model with the tool path, and an experiment is carried out for validation. Results show the simulation surface is highly consistent with the experimental result. Dynamic performance of the spindle is the main factor for texture generation, and optimization of spindle is investigated, DFEA of the optimized spindle shows better performance, and the connection mode between diamond tool and cutter head should be further studied.

✉ Chenhui An
hplaser@126.com

Xu Yang
yxcrab@163.com

Zhenzhong Wang
wangzhenzhong@xmu.edu.cn

Quanjin Wang
wqjsimple@163.com

Yunfeng Peng
pengyf@xmu.edu.cn

Jian Wang
wj7130@sina.com

[1] Chengdu Fine Optic Engineering Research Center, Chengdu 610041, China

[2] Department of Mechanical and Electrical Engineering, Xiamen University, Xiamen 361005, China

Keywords Ultra-precision cutting · Air spindle · Dynamic performance · DEFA · Surface topography

Nomenclature

O_T-$x_Ty_Tz_T$	Actual tool coordinate system
O-xyz	Workpiece coordinate system
O_S-$x_Sy_Sz_S$	Ideal tool coordinate system
r	Radius of cutting edge
θ	Rake angle of diamond tool
φ	Position angle of point P on cutting edge
R	Radius of cutter head
W	Width of workpiece
L	Length of workpiece
t	Machining time
n	Spindle speed
f	Feed rate
α	Position angle of tool center O_S
R_S	Rotation matrix from coordinate system O_S-$x_Sy_Sz_S$ to O-xyz
T_T	Translation matrix from coordinate system O_T-$x_Ty_Tz_T$ to O_S-$x_Sy_Sz_S$
R_T	Rotation matrix from coordinate system O_T-$x_Ty_Tz_T$ to O_S-$x_Sy_Sz_S$
Δx_T	Amplitude of tool center in O_Sx_S direction
Δy_T	Amplitude of tool center in O_Sy_S direction
Δz_T	Amplitude of tool center in O_Sz_S direction
Δx_S	Tool offset error along O_Sx_S axis
β	Error angle between ideal tool coordinate system O_S-$x_Sy_Sz_S$ and actual tool coordinate system O_T-$x_Ty_Tz_T$

1 Introduction

Ultra-precision cutting was developed with single point diamond turning (SPDT), which could achieve micro-nano surface roughness with air spindle, pneumatic slide, high-stiffness, and high-accuracy tool, feedback control, and temperature control [1]. Currently, SPDT is wildly used in the fields of aerospace, national defense, astronomy, and laser fusion to obtain reflector, sphere, and aspherical elements of large size [2–4]. It has become the main machining method for some soft, frangible, and deliquescence optical crystal [5, 6]. Besides, soft metals, such as aluminum and copper, are machined by SPDT generally [7, 8].

Realizing ultra-precision machining is achieving micro removal of the material, and the first condition is ultra-precision machine tool. It needs not only shape tools or fine abrasives, but also good dynamic performance and high-accuracy micro feed system more importantly [9, 10], as the direct and hard contact between tool and work-piece in machine work, the vibration of machine tool is easy to reflect on the machined surface. To date, some researchers have studied the dynamic performance of ultra-precision cutting machine tool; Liang et al. [11] presented a dynamic optimization of an ultra-precision diamond flycutting machine tool, successfully produced 415 × 415-mm surfaces on aluminum and crystalline optics, with 1.3-μm flatness and 2.4-nm rms roughness. Sun et al. [12] studied a dynamic error budget methodology designing and characterizing machines used to manufacture or inspect parts with spatial frequency-based specifications. In the two researches, they both studied the dynamic performance of the whole machine tool, and the max deformation of the machine almost occurred on the air spindle, however, they did not take further study on the spindle.

As the key part of ultra-precision cutting machine tool, air spindle could affect the machining quality directly. Akhondzadeh and Vahdati [13] studied the variable depth air pockets to low the vibrations of spindle in ultra-precision machine tools. But structure of the air spindle also has influences on its vibrations. This paper concentrates on the effects of dynamic performance of air spindle on the machining accuracy of the ultra-precision machine tools developed by Harbin Institute of Technology, and gets optimization tips.

2 Surface topography model for flycutting

In this paper, ultra-precision machine tool consists of air spindle, diamond tool, liquid floating skateboard, vacuum chuck, marble base, and column beam. During the machining process, work-piece is adsorbed on the surface of vacuum chuck, and moving with the liquid skateboard, while diamond tool speed rotating with air spindle and cutting the work-piece, as shown in Fig. 1. Generally, only one diamond tool is used in machining process, and a bob-weight tool is installed on another cutter frame to keep the balance of the air spindle.

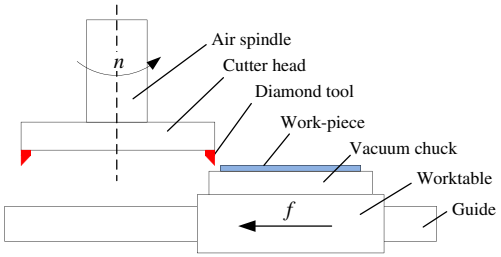

Fig. 1 Diagrammatic map of flycutting machining

The cutting edge of the diamond tool is presented in Fig. 2, it is arc-shaped, whose radius is r, tool coordinate system is built by setting the center of the cutting edge as coordinate origin as shown in Fig. 2, where Q is the midpoint of the cutting edge, and P is an arbitrary point on the cutting edge, the coordinates of P are calculated as Eq. 1.

$$\begin{cases} x_{Pi} = r\cos\varphi\sin\theta \\ y_{Pi} = r\sin\varphi \\ z_{Pi} = -r\cos\varphi\cos\theta \end{cases} \tag{1}$$

Where, r is the radius of cutting edge, and $r = 6$ mm, θ is the negative rake angle of diamond tool, and $\theta = 45$ degree, φ is the position angle of point P on cutting edge.

According to the machining mechanism of flycutting (Fig. 1), work-piece coordinate system is built as shown in Fig. 3. In this system: (a) Oz axis is coincide with the axis of air spindle, (b) plane xOy is coincide with cutting surface, (c) Oy is the opposite direction of feeding. Through the position relationship between tool and work-piece, the coordinates of ideal center of cutting edge O_S in work-piece coordinate system are shown as Eq. 2.

$$\begin{cases} x_S = R\sin\alpha \\ y_S = ft + R\cos\alpha\,,\ \alpha = \arcsin\left(\dfrac{W}{2R}\right) - \dfrac{2\pi n}{60}t \\ z_S = r\cos\theta \end{cases} \tag{2}$$

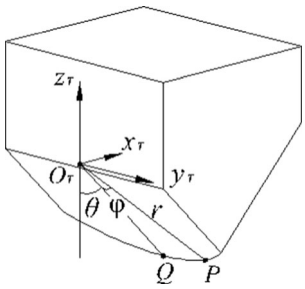

Fig. 2 Cutting edge model of a diamond tool

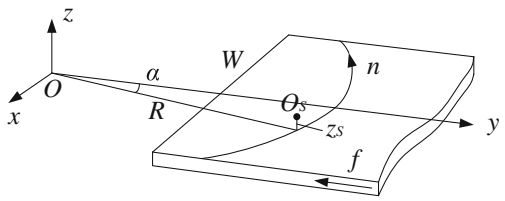

Fig. 3 Workpiece coordinate system

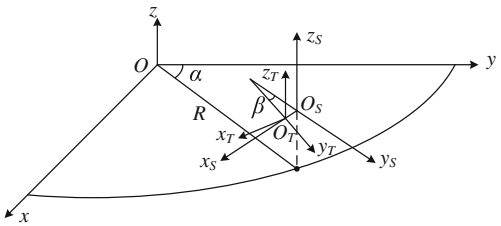

Fig. 4 Model of coordinate transformation

Where, R is the radius of cutter head, and $R = 325$ mm, W is the width of work-piece, t is the machining time, n is the spindle speed (rpm), f is the feed rate, r is the radius of cutting edge, θ is the negative rake angle of diamond tool, and α is the position angle of tool center O_S.

In the machining process, the diamond tool is manually installed, and installation error could not be avoided, it is assumed the tool has an offset Δx_S along $O_S x_S$ axis and a deflection angle β around the $O_S z_S$ axis. Therefore, the position relationship among work-piece coordinate system O-xyz, ideal tool coordinate system O_S-$x_S y_S z_S$ and actual tool coordinate system O_T-$x_T y_T z_T$ can be presented as Fig. 4.

According to the principle of coordinate transformation, coordinates of point P in work-piece coordinate system can be obtained by Eq. 3.

$$\begin{bmatrix} x_i \\ y_i \\ z_i \\ 1 \end{bmatrix} = \begin{bmatrix} x_S \\ y_S \\ z_S \\ 1 \end{bmatrix} + R_S T_T R_T \begin{bmatrix} x_{Pi} + \Delta x_T \\ y_{Pi} + \Delta y_T \\ z_{Pi} + \Delta z_T \\ 1 \end{bmatrix} \tag{3}$$

Where, Δx_T, Δy_T, Δz_T are the vibration values of tool center in $O_S x_S$, $O_S y_S$, $O_S z_S$ direction respectively, R_S is rotation matrix from coordinate system O_S-$x_S y_S z_S$ to O-xyz, T_T, and R_T are translation matrix and rotation matrix from coordinate system O_T-$x_T y_T z_T$ to O_S-$x_S y_S z_S$ respectively, and

$$R_S = \begin{bmatrix} \cos\alpha & \sin\alpha & 0 & 0 \\ -\sin\alpha & \cos\alpha & 0 & 0 \\ 0 & 0 & 1 & 0 \\ 0 & 0 & 0 & 1 \end{bmatrix} \tag{4}$$

$$T_T = \begin{bmatrix} 1 & 0 & 0 & \Delta x_S \\ 0 & 1 & 0 & 0 \\ 0 & 0 & 1 & 0 \\ 0 & 0 & 0 & 1 \end{bmatrix} \tag{5}$$

$$R_T = \begin{bmatrix} \cos\beta & \sin\beta & 0 & 0 \\ -\sin\beta & \cos\beta & 0 & 0 \\ 0 & 0 & 1 & 0 \\ 0 & 0 & 0 & 1 \end{bmatrix} \tag{6}$$

Where, Δx_S is the offset error along $O_S x_S$ axis, β is the error angle between ideal tool coordinate system O_S-$x_S y_S z_S$ and actual tool coordinate system O_T-$x_T y_T z_T$.

In the flycutting process, tool paths of cutting edge form the surface topography of work-piece. Therefore, surface topography would be obtained by Eq. 3 if the vibration values of tool center were achieved.

3 Tool path acquirement based on DFEA of air spindle

Dynamic finite element analysis (DFEA) of air spindle is conducted in ANSYS Workbench to obtain the vibration displacement of diamond tool when the tool is cutting the work-piece. In the machining process, surface quality is sensitive to the displacement of the tool in z direction, and cutting force in z direction is the main force, to simplify the question, only cutting force in z direction is considered in DFEA of the air spindle. The map of cutting force of an optical crystal in z direction is shown in Fig. 5, which is measured by Kistler 9255C dynamometer. Obviously, there exists an impact while the tool cutting on the work-piece, cutting force gets a large value firstly, and then decreases until the tool cutting out the work-piece. For aluminum mirror, the cutting force is bigger, it is assumed 1.5 N when feed rate is 40 μm/r, cutting depth is 10 μm [14]. Based on the above analysis, transient analysis parameters are chosen as Table 1, and the finite element model (FEM) of the air spindle is built as Fig. 6.

Figure 7 shows the deformation map of the air spindle in the machining process, it indicates that deformation of the air spindle mainly occurred on the cutter head, and the deformation of tool installation position is the largest.

Figure 8 shows the vibration curves of the tool center in x, y, and z direction, it shows the displacement in z direction is the largest, follows x direction, and deformation in y direction

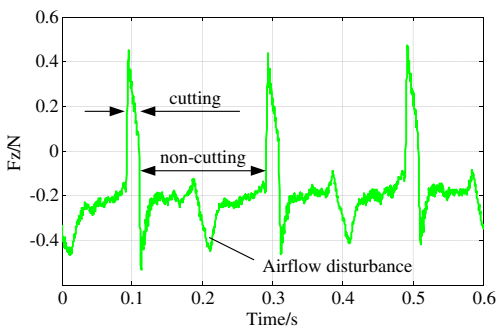

Fig. 5 Cutting force in z direction

Table 1 Parameters for DFEA

Parameters	Values
Spindle speed n (rpm)	300
Feed rate f (μm/s)	200
Cutting depth a_p (μm)	10
Air spindle pressure P (MPa)	0.5
Cutting force in z direction F_z (N)	1.5–1.3
Cutting time t (ms)	5

is the smallest, it is less than 0.085 nm, which can be ignored, so $\Delta y_T = 0$. The principle of least squares (LS) is used to fit the vibration curves of tool center in the x and z direction, the fitted equation is shown as Eq. 7. From Fig. 8, the fitted curves are well coincide with the vibration curves, the R-squared value and adjusted R-squared value are bigger than 0.99, the equation is available.

$$\begin{cases} \Delta x_T = 20.91\sin(0.6474t - 0.3921) + 11.75\sin(1.296t + 0.6906) \\ \quad +4.199\sin(3.889t - 2.335) + 1.91\sin(2.592t + 0.6781) \\ \quad +0.9329\sin(6.471t - 1.666) + 0.3795\sin(10.37t - 2.404) \\ \quad +0.2414\sin(7.727t + 1.332) \\ \Delta y_T = 0 \\ \Delta z_T = 26.2\sin(0.6473t - 0.3731) + 14.54\sin(1.295t + 0.7524) \\ \quad +6.055\sin(3.886t - 2.323) + 2.682\sin(2.591t + 0.5291) \\ \quad +0.498\sin(6.487t - 1.916) + 0.2668\sin(7.772t + 1.316) \\ \quad +0.2693\sin(5.182t + 1.858) + 0.1376\sin(10.37t - 2.367) \end{cases} \quad (7)$$

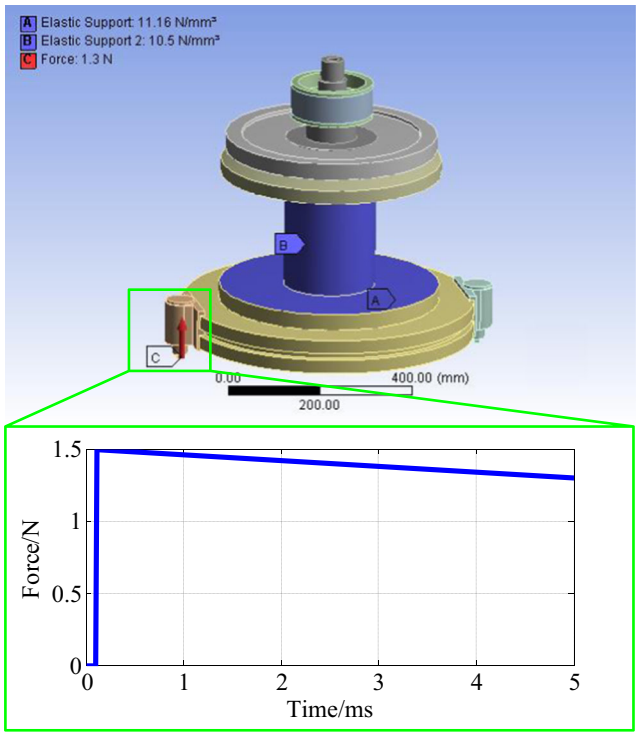

Fig. 6 FEM of air spindle in DFEA

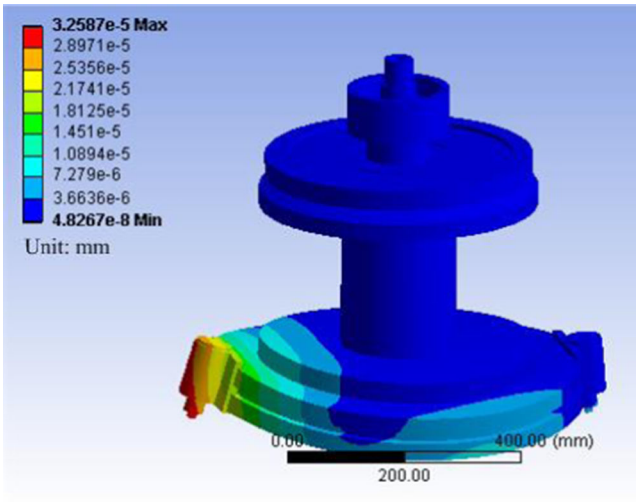

Fig. 7 Deformation map of the air spindle

Where Δx_T, Δy_T, Δz_T are the vibration values of tool center in $O_S x_S$, $O_S y_S$, $O_S z_S$ direction respectively, t is the machining time unit millisecond, the unit of phases in the equation is rad.

4 Surface simulation and experiment

Surface simulation is conducted in MATLAB by combining tool vibration equation (Eq. 7) with surface topography model (Eq. 3), simulation parameters are presented in Table 2. The width of work-piece in simulation is 50 mm, which is the length of tool moving in 5 ms (it is the time of transient analysis), the length of work-piece in simulation is 8 mm considering the calculate efficiency of PC and it is a repeat process along the feeding direction, the simulation process is shown in Fig. 9.

Figure 10 shows the simulation result (cutting start from the right hand of the picture), there are three stripes appeared on the surface sized 50 mm × 8 mm, and the stripe in the middle of the surface is narrower, the spaces between the three stripes are 15 and 18 mm, respectively, from the cutting side.

Experiment is carried out on an aluminum mirror sized 410 mm × 410 mm to verify the simulation results, the machining parameters are the same as simulation parameters presented in Table 2. Machine tool is a 650 mm-aperture ultra-precision flycutting machine tool, ZYGO-32″ plane interferometer is used to observe the machining surface, whose horizontal resolution is 0.8 mm/pix, and cavity detection accuracy is 1/10λ (λ = 632.8 nm), that satisfies the testing accuracy entirely.

Figure 11 demonstrates the experimental result, and cutting side is on the right of the figure. There exists significant texture on the surface. For further study, the area width 50 mm

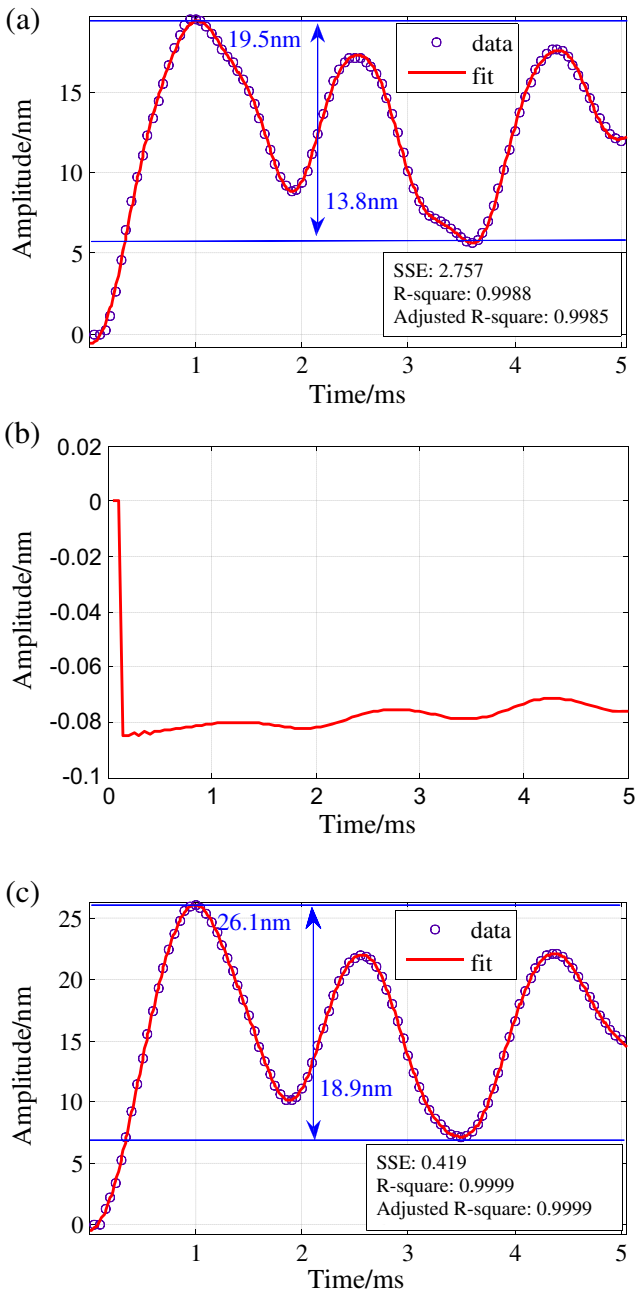

Fig. 8 Vibration curves of the tool center

besides cutting edge (the red rectangular area in Fig. 11) is taken out as shown in Fig. 12.

5 Results and analysis

Figures 11 and 12 shows there are stripes along the cutting direction on the surface, and three stripes appear in the range of 50 mm about the cutting side, the distance between the stripes are 14.9 and 18.1 mm from the X profile of the surface as shown in Fig. 12a, b. The result is consistent with the simulation result, the surface topography model and transient analysis is verified.

Table 2 Parameters for surface simulation

Parameters	Values
Spindle speed n (rpm)	300
Feed rate f (μm/s)	200
Cutting depth a_p (μm)	10
Cutting edge radius r (mm)	6
Tool rake angle θ (degree)	45
Cutter head radius R (mm)	325
Work-piece width W (mm)	50
Work-piece length L (mm)	8
Air spindle pressure P (MPa)	0.5
Offset error of tool Δx_S (μm)	10
Error angle of tool β (degree)	0.5

On the other hand, the experimental amplitude is larger than the simulation value obviously, there are three reasons: (a) Cutting force only in z direction is considered in DFEA, although which in x and y direction has little effect on the surface. (b) The airflow caused by the rotation of spindle is not taken into consideration while it has made a difference on cutting force as shown in Fig. 5. (c) Vibration of worktable is

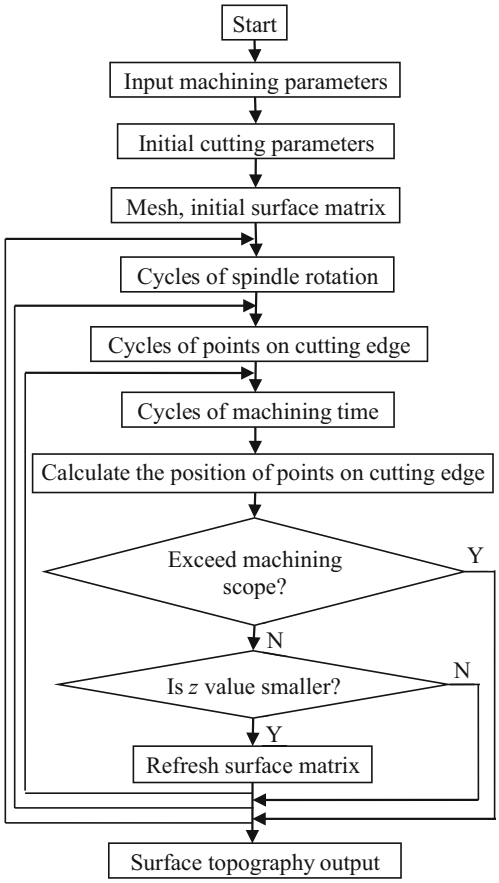

Fig. 9 Surface simulation process

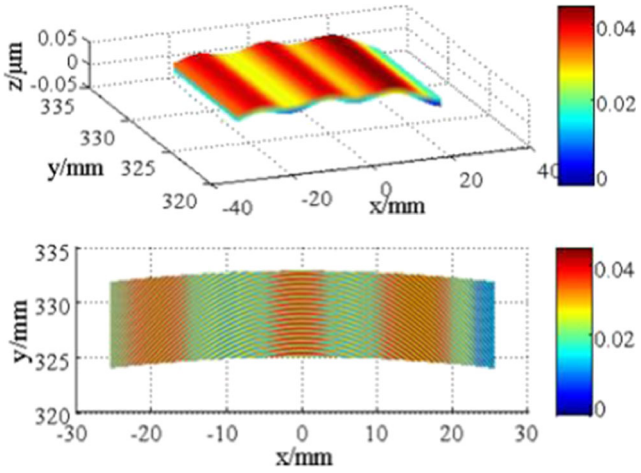

Fig. 10 Surface simulation result

ignored. The simulation surface still approach to the experimental result apart from those factors, and the dynamic performance is the main factor for the generation of stripes on the surface.

Stripes on the surface have great influence on life and property of the element. In terms of optical elements, the texture will have a great gain under glare nonlinear effects, and then convert to great intensity modulation after a long-distance transmission, and a poor beam quality is generated, laser damage is also more possible to occur [15]. Therefore, optimization of the air spindle is essential.

From DFEA result in Fig. 7, deformation of the air spindle focuses on cutter head during the machining process, so the stiffness of cutter head is to be strengthened, such as increasing its thickness or using the materials with higher stiffness.

Figure 13 shows the optimization of the cutter head, four rids are crosswise added under the cutter head where the deformation occurred to increase its stiffness based on the deformation map in Fig. 7. DFEA of the new cutter head is carried out afterwards to estimate the optimization effect. According to the principle of single variable, the simulation parameters are the same as Table 1.

Figure 14 demonstrates the deformation graph of the new spindle, the deformation shape of the spindle almost the same as shown in Fig. 7, but the deformation value reduced a lot.

Figure 15 shows the vibration curves of the tool center after optimization, to better estimate the effects of optimization, Table 3 shows the vibration parameters of original and optimized cutter head, as can be seen from the result, vibration amplitude of new cutter head has a substantial reduction in x and z direction, they maximum vibration amplitudes reduced 46.7 and 43.2 %, respectively, after optimization, but the amplitude in y direction has little difference. What is more, the fluctuation ranges of the vibration curves also reduced a lot, the range changes from 13.8 to 7.4 nm in x direction, and reduces from 18.9 to 8.9 nm in z direction, which also decreased in y direction, that would low the amplitude of stripes on the surface. The optimization has achieved significant effects.

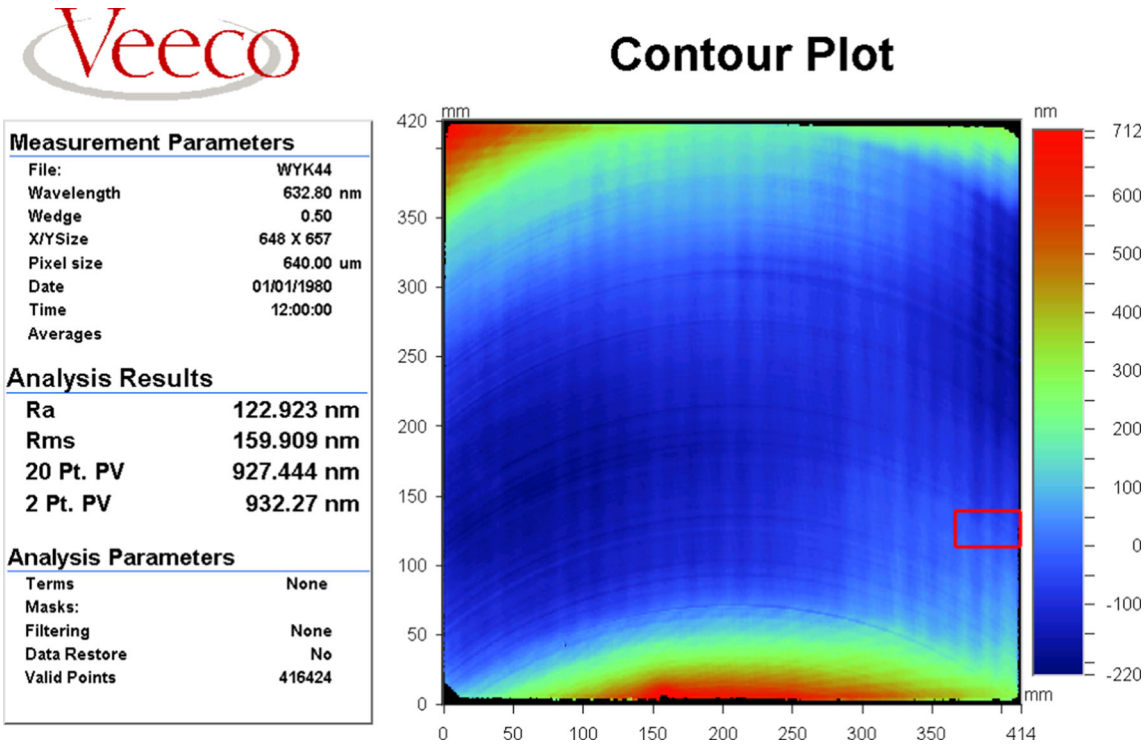

Fig. 11 Whole surface topography of work-piece

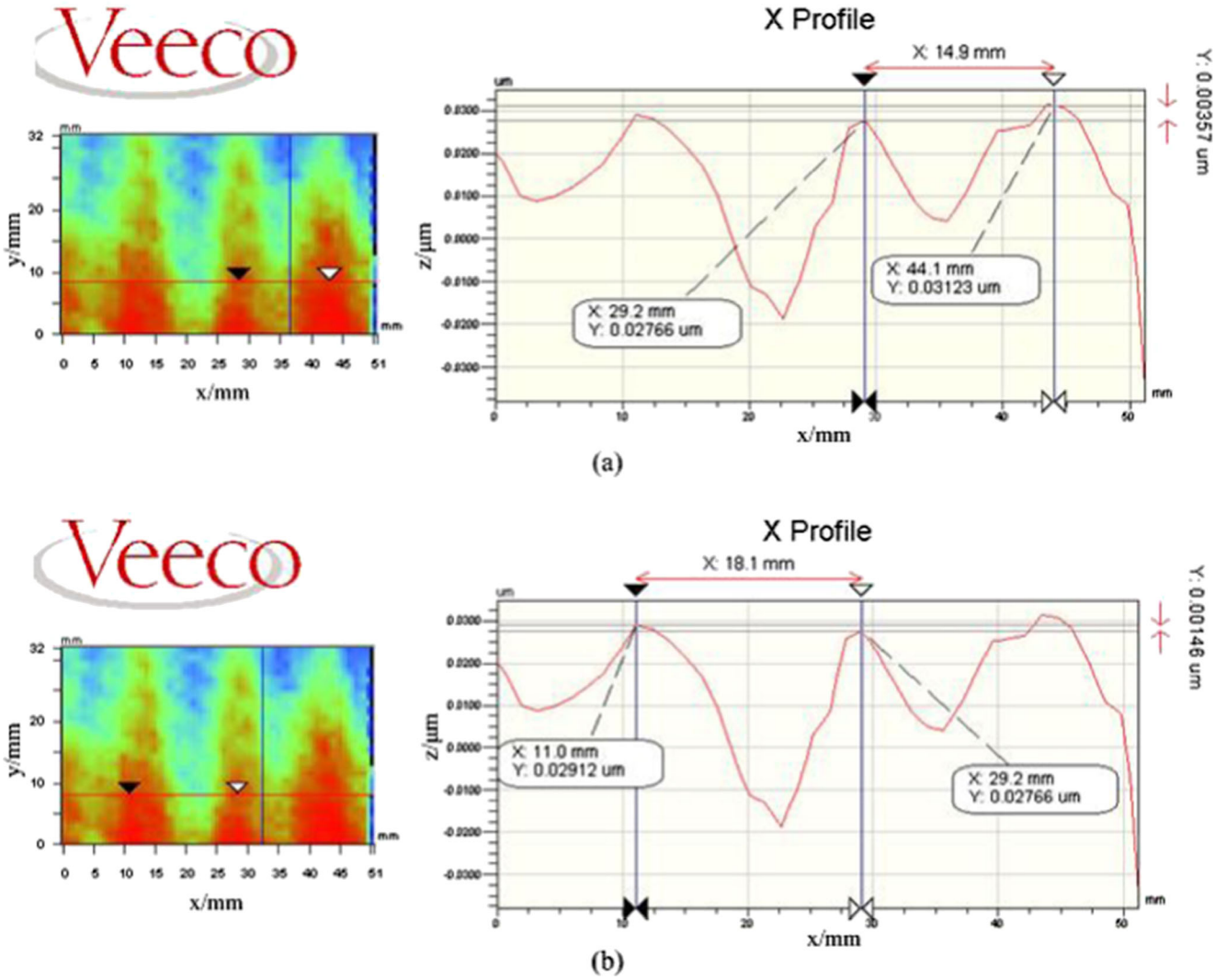

Fig. 12 Local surface topography width 50 mm

To further curb the surface streaks, the connection mode between cutter head and diamond tool should be studied based on the deformation shape in Fig. 14.

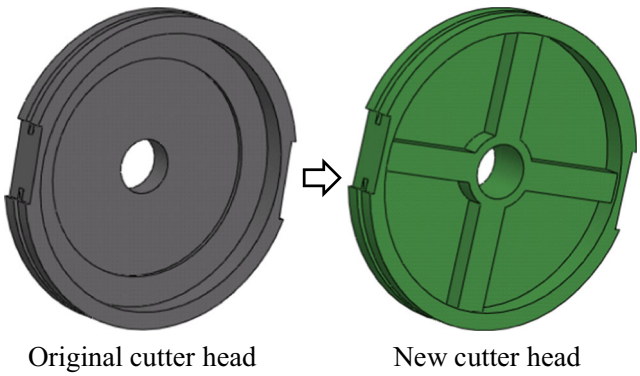

Fig. 13 Optimization of the cutter head

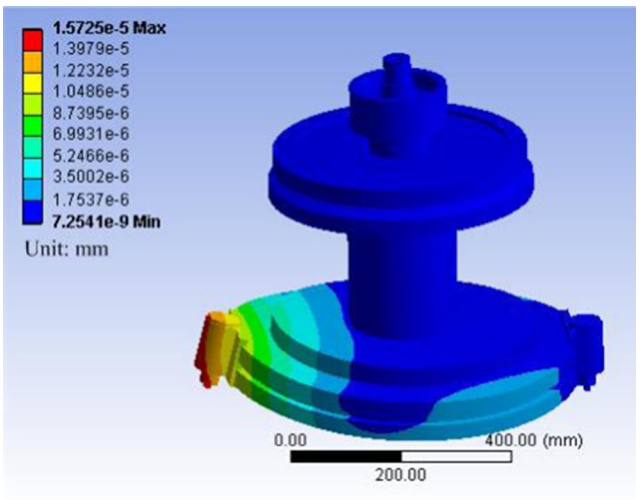

Fig. 14 Deformation graph of the air spindle with new cutter head

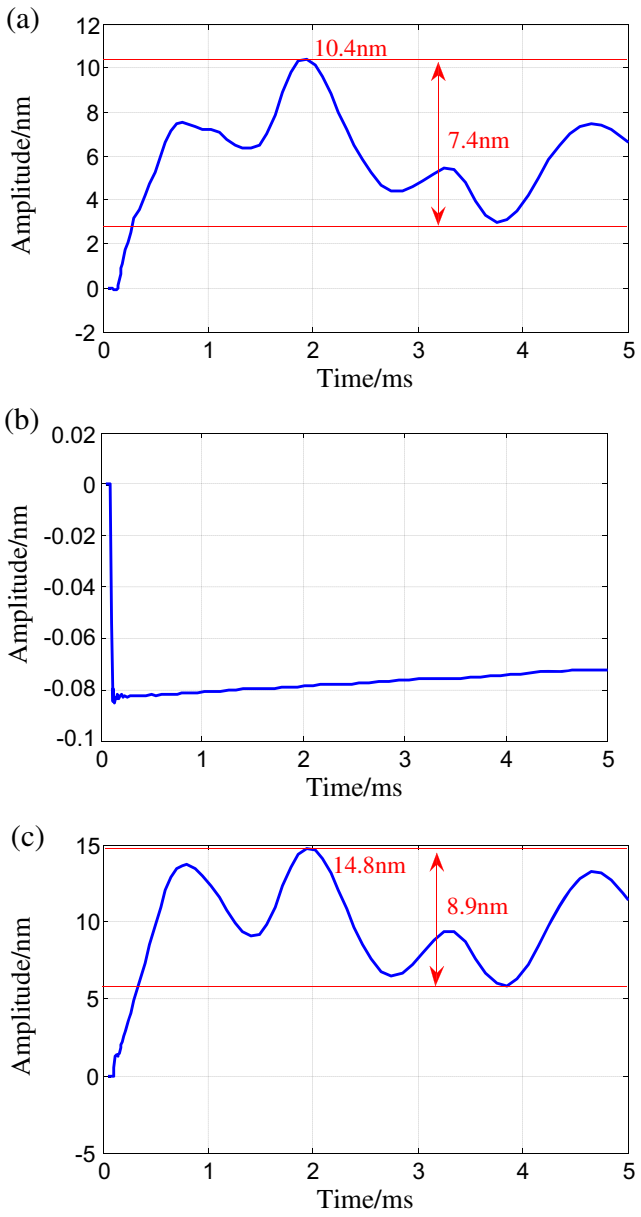

Fig. 15 Vibration curves of tool center after optimization

6 Conclusions

Dynamic performance of the ultra-precision machine tool has great influence on the surface quality. Through simulation and experiment on the surface morphology, three conclusions are summarized:

(a) Surface topography model is built for ultra-precision flycutting, and it has good predictive ability.
(b) Dynamic characteristics of the air spindle are the main factor for the generation of strips on the surface.
(c) After enhancing the stiffness of the cutter head, the displacement of the tool center significantly reduced from the result of DFEA, and the surface morphology is expected to be improved. To further curb the surface streaks, the connection mode between cutter head and diamond tool should be studied.

Apart from that, the effects of airflow and worktable on surface quality are to be reported in later researches.

Table 3 Comparison of vibration characteristics between original and optimized cutter head

Vibration parameters	Original		Optimized	
	x	*z*	*x*	*z*
Max amplitude (nm)	19.5	26.1	10.4	14.8
Fluctuation range (nm)	13.8	18.9	7.4	8.9

Compliance with ethical standards

Grant Ultra-precision Machining Technology Key Laboratory Major Fund of China Academy of Engineering Physics (Grant No. ZZ14002)

References

1. Komanduri R, Lucca DA, Tani Y (1997) Technological advances in fine abrasive process. Ann CIRP 46(2):545–595
2. Taniguchi N (1983) Current status in and future trends of ultraprecision machining and ultrafine materials processing. Ann CIRP 32(2):573–582
3. Tian FJ, Yin ZQ, Li SY (2015) Fast tool servo diamond turning of optical freeform surfaces for rear-view mirrors. Int J Adv Manuf Technol 80(9–12):1759–1765
4. Kim HC, Lee SG (2012) Development of machining technology for micropatterns with large surface area. Int J Adv Manuf Technol 58(9):1261–1270
5. Kaishi SK (1998) Single point diamond turning of KDP inorganic non-linear optical crystal for laser fusion. J Japan Soc Precis Eng 64(10):1181–1185
6. Jasinevicius RG, Pizani PS, Cirino GA (2015) Ultraprecision machining of diffraction optical elements on soft semiconductor crystal. Int J Adv Manuf Technol 77(5–8):1145–1154
7. Pramanik A, Littlefair G (2015) Developments in machining of stacked materials made of CFRP and titanium/aluminum alloys. Mach Sci Technol 18(4):485–508
8. Tanaka H, Shimada S, Higuchi M, Yamaguchi T, Kaneeda T, Obata K (2005) Mechanism of cutting edge chipping and its suppression in diamond turning of copper. CIRP Ann Manuf Technol 54(1):51–54
9. Yuan JL, Zhang FH, Dai YF, Kang RK, Yang H, Lü BH (2010) Development research of science and technologies in ultra-precision machining field. J Mech Eng 15(46):161–177, In Chinese
10. Biju CV, Shunmugam MS (2014) Investigation into effect of particle impact damping (PID) on surface topography in boring operation. Int J Adv Manuf Technol 75(5):1219–1231
11. Liang YC, Chen WQ, Bai QS, Sun YZ, Chen GD, Zhang Q, Sun Y (2013) Design and dynamic optimization of an ultraprecision

diamond flycutting machine tool for large KDP crystal machining. Int J Adv Manuf Technol 69(237):244
12. Sun YZ, Chen WQ, Liang YC, An CH, Chen GD, Su H (2015) Dynamic error budget analysis of an ultraprecision flycutting machine tool. Int J Adv Manuf Technol 76(1215):1224
13. Akhondzadeh M, Vahdati M (2014) Study of variable depth air pockets on air spindle vibrations in ultra-precision machine tools. Int J Adv Manuf Technol 73(5):681–686
14. Khajehzadeh M, Razfar MR (2015) FEM and experimental investigation of cutting force during UAT using multicoated inserts. Mater Manuf Process 30(7):858–867
15. Chen MJ, Li MQ, Jiang W, Xu Q (2010) Influence of period and amplitude of micro-waviness on KH2PO4 crystal's laser damage threshold. J Appl Phys 108(4):043109